On-site secretory vesicle delivery drives filamentous growth in the fungal pathogen Candida albicans

Allon Weiner, François Orange, Sandra Lacas-Gervais, Katya Rechav, Vikram Ghugtyal, Martine Bassilana, Robert Arkowitz

HAL Id: hal-02366663
https://hal.archives-ouvertes.fr/hal-02366663

RESEARCH ARTICLE

WILEY

On-site secretory vesicle delivery drives filamentous growth in the fungal pathogen *Candida albicans*

Allon Weiner[1] | François Orange[2] | Sandra Lacas-Gervais[2] | Katya Rechav[3] | Vikram Ghugtyal[1] | Martine Bassilana[1] | Robert A. Arkowitz[1] [ID]

[1] Université Côte d'Azur, CNRS, Inserm, Institute of Biology Valrose, Parc Valrose, Nice, France

[2] Université Côte d'Azur, CCMA, Parc Valrose, Nice, France

[3] Chemical Research Support, Weizmann Institute of Science, Rehovot, Israel

Correspondence
Robert A. Arkowitz, Institute of Biology Valrose, Université Côte d'Azur, CNRS, Inserm, Parc Valrose, Nice, France.
Email: arkowitz@unice.fr

Funding information
Centre National de la Recherche Scientifique; European Union H2020 Marie Skłodowska-Curie Actions, Grant/Award Number: MSCA-ITN-2015-ETN-GA-675407; Ville de Nice postdoctoral fellowship; Agence Nationale de la Recherche, Grant/Award Numbers: ANR-11-LABX-0028-01 and ANR-16-CE13-0010-01

Abstract

Candida albicans is an opportunistic fungal pathogen that colonises the skin as well as genital and intestinal mucosa of most healthy individuals. The ability of *C. albicans* to switch between different morphological states, for example, from an ellipsoid yeast form to a highly polarised, hyphal form, contributes to its success as a pathogen. In highly polarised tip-growing cells such as neurons, pollen tubes, and filamentous fungi, delivery of membrane and cargo to the filament apex is achieved by long-range delivery of secretory vesicles tethered to motors moving along cytoskeletal cables that extend towards the growing tip. To investigate whether such a mechanism is also critical for *C. albicans* filamentous growth, we studied the dynamics and organisation of the *C. albicans* secretory pathway using live cell imaging and three-dimensional electron microscopy. We demonstrate that the secretory pathway is organised in distinct domains, including endoplasmic reticulum membrane sheets that extend along the length of the hyphal filament, a sub-apical zone exhibiting distinct membrane structures and dynamics and a Spitzenkörper comprised of uniformly sized secretory vesicles. Our results indicate that the organisation of the secretory pathway in *C. albicans* likely facilitates short-range "on-site" secretory vesicle delivery, in contrast to filamentous fungi and many highly polarised cells.

1 | INTRODUCTION

Candida albicans is a human fungal pathogen that switches between an oval yeast form and a filamentous hyphal form, a transition which is critical for virulence (Moyes, Richardson, & Naglik, 2015). This morphological transition is accompanied, in particular, by changes in the cell wall that are critical for host immune responses (Gow & Hube, 2012; Hall & Gow, 2013; Lewis et al., 2012; Pericolini et al., 2018; Wheeler, Kombe, Agarwala, & Fink, 2008). In susceptible hosts, *C. albicans* can penetrate the gastrointestinal mucosa and enter the bloodstream leading to severe systemic infection (Pfaller & Diekema, 2010). Host tissue penetration and damage by *C. albicans* is, in particular, promoted by growing hyphae, which produce lytic enzymes such as secreted aspartic proteases and peptide toxins such as candidalysin (da Silva Dantas et al., 2016; Höfs, Mogavero, & Hube, 2016; Moyes et al., 2016; Naglik, König, Hube, & Gaffen, 2017). Tissue invasion also results from active penetration of both oral and intestinal epithelia by growing hyphae (Dalle et al., 2010; Moyes et al., 2015; Naglik et al., 2017; Phan et al., 2007). The molecular processes driving *C. albicans* filamentous growth have been extensively studied, demonstrating that a tight spatio-temporal regulation of exocytosis and endocytosis is required for this process (Bar-Yosef et al., 2018; Bishop et al., 2010; Guo, Yong, Wang, & Li, 2016; Labbaoui et al., 2017; Li, Lee, Wang, Zheng, & Wang, 2007; Martin et al., 2007; Zeng, Wang, & Wang, 2012), ultimately resulting in the regulated fusion of secretory vesicles (SVs) with the apical plasma membrane (PM), alongside endocytosis from sites located just behind the apex of the filamentous cell (Anderson & Soll, 1986; Caballero-Lima, Kaneva, Watton, Sudbery, & Craven, 2013; Ghugtyal et al., 2015). SVs at the apex form a structure known as the Spitzenkörper (Spk), which is thought to act as a vesicle supply centre regulating filamentous growth (Bartnicki-Garcia, Bartnicki, Gierz, López-Franco, & Bracker, 1995), though its precise structure and function are not well understood.

Other highly polarised tip-growing cells such as neurons, pollen tubes, root hairs, and filamentous fungi have evolved distinct mechanisms that are responsible for the long-range delivery of membrane and cargo to their tip. In these cells, the long-range delivery of SVs tethered to motors moving along cytoskeletal cables, from the cell body to the growing tip, appears to be a common feature of secretory pathway organisation (Geitmann & Emons, 2000): in axons, trafficking of membrane bound cargo occurs via kinesins and dynein moving along longitudinally arranged microtubules (MTs), a mechanism known as fast axonal transport (González & Couve, 2014). Pollen tube growth relies on extensive networks of long actin cables and MTs, which together with their associated motors facilitate the transport of cargo throughout the shank of the tube (Chebli, Kroeger, & Geitmann, 2013). In the filamentous fungus *Aspergillus nidulans*, transport occurs via a relay mechanism whereby SVs are moved along MTs by kinesins from apex-distal regions to the hyphal tip, where they are handed over to myosin-5 that transports them along actin cables to the PM (Pantazopoulou, Pinar, Xiang, & Peñalva, 2014). In another filamentous fungus, *Neurospora crassa*, MTs are longitudinally arranged along the length of the hyphae with a helical curvature, with dynein and dynactin implicated in SV transport to the hyphal tip (Mouriño-Pérez, Riquelme, Callejas-Negrete, & Galván-Mendoza, 2016). Interestingly, an alternative secretory pathway organisation that allows long-range delivery of membrane and cargo to the apex of the filamentous cell has been reported in neurons of the visual system of *Drosophila* (Yogev, Schejter, & Shilo, 2010). The epidermal growth factor receptor ligand Spitz (Spi) is transported from the cell body through the ER to the axonal terminus, where it is secreted via short-range on site transport of SVs towards the PM through a currently poorly understood mechanism (González & Couve, 2014).

The process of *C. albicans* polarised growth presents several common features with filamentous fungi: the presence of a Spk, endocytosis via actin patches located sub-apically (Berepiki, Lichius, & Read, 2011; Caballero-Lima et al., 2013; Ghugtyal et al., 2015; Martin et al., 2007), scattered (nonstacked) Golgi cisternae (Harris, 2013; Rida, Nishikawa, Won, & Dean, 2006) and the requirement for intact actin cables required for motor mediated trafficking of cargo and membranes towards the apex (Berepiki et al., 2011; Crampin et al., 2005; Jones & Sudbery, 2010). It is therefore generally assumed that the principles of polarised growth in *C. albicans* are similar to those found in filamentous fungi such as *N. crassa* and *A. nidulans*. However, a key difference suggests that perhaps this view is oversimplified. *C. albicans* filamentous growth is not dependent on MTs (Rida et al., 2006), a central feature in *N. crassa* and *A. nidulans* filamentous growth. In addition, *C. albicans*'s ability to switch from yeast to hyphal form, its smaller filament diameter, and its substantially lower rate of hyphal extension further set it apart from filamentous fungi. These differences may reflect the presence of unique polarised growth mechanisms in *C. albicans*, particularly in relation to the organisation of its secretory pathway.

Here, we employed dynamic imaging and three-dimensional (3D) electron microscopy to study the organisation of the secretory pathway of *C. albicans* during filamentous growth in detail. We provide the first high-resolution view of the *C. albicans* Spk and demonstrate that the secretory pathway along hypahe is organised in distinct dynamic and structural domains, suggesting that short-range SV transport is a major feature of filamentous growth. Our results reveal a unique feature of *C. albicans* polarised growth compared with filamentous fungi and highlight the emerging concept of on-site vesicle delivery mechanisms in a subclass of highly polarised cells.

2 | RESULTS AND DISCUSSION

2.1 | SVs in *C. albicans* filamentous cells are differentially distributed in distinct regions

The Rab GTPase Sec4 localises to the *C. albicans* Spk together with the myosin light chain Mlc1, (Crampin et al., 2005; Jones & Sudbery, 2010; Li et al., 2007) and is also observed on SVs throughout the filamentous cell (Ghugtyal et al., 2015). Sec4 is important for growth, as a dominant negative mutant inhibits growth and results in the accumulation of SVs (Mao, Kalb, & Wong, 1999). Its distribution is altered in the Arf GTPase *arl1* mutant, which exhibits slower hyphal filament extension rate (Labbaoui et al., 2017; Wakade, Labbaoui, Stalder, Arkowitz, & Bassilana, 2017) suggesting the importance of SV traffic through the Spk. *C. albicans* cells lacking the exocyst subunit Sec3 can form germ tubes but are unable to maintain tip growth, accumulating SVs at the tip which swells over time, consistent with reduced SV fusion at the apical PM (Li et al., 2007). Together, these results indicate the importance of SV traffic and fusion at the Spk and apical PM. SVs originate from Golgi cisternae, which have been previously shown to redistribute towards the tip of the filamentous cell (Rida et al., 2006). However, closer examination of the Golgi marker FAPP1 (four-phosphate-adaptor protein 1) revealed that in cells with a ~10 μm long filament, around half of the cisternae are found in mother cell and half in the hyphal filament (Figure 1a,b; Movie S1). This observation raises the question as to whether SVs are delivered to the hyphal tip via long-range transport along cytoskeletal tracks, as observed in other filamentous fungi or via a novel mechanism.

We therefore set out to examine the pattern of SV dynamics in *C. albicans* filamentous cells of a similar length (Figure 1c,d; Movie S2). Our results demonstrate that GFP-Sec4 is distributed in three distinct regions along the hyphal filament: in agreement with previous studies (Ghugtyal et al., 2015; Jones & Sudbery, 2010), Sec4 is predominantly localised to the Spk (Segment 10, 0.41 ± 0.10 total signal) and is also present on vesicles along the entire length of the hyphal filament (Segments 1–7, 0.40 ± 0.15 total signal). Surprisingly, analysis also revealed a region located just behind the hyphal apex, where Sec4-GFP intensity was intermediate between that of the Spk and that found along the hyphal filament length (Segments 8–9, 0.19 ± 0.03 total signal). GFP-Sec4 in this distinct region was highly dynamic, showing multiple localisation patterns over the course of a time lapse (see Figure 1c kymograph and Movie S2). Sub-apical regions (SARs) possessing specific functions have been reported in other highly polarised cells, for example, a relay area in *A. nidulans* where SVs transition from MT to actin mediated transport (Pantazopoulou et al., 2014; Peñalva, Zhang, Xiang, & Pantazopoulou, 2017), and an area devoid of organelles termed the "clear zone" in tobacco and lily pollen tubes, where a transition from apical transport
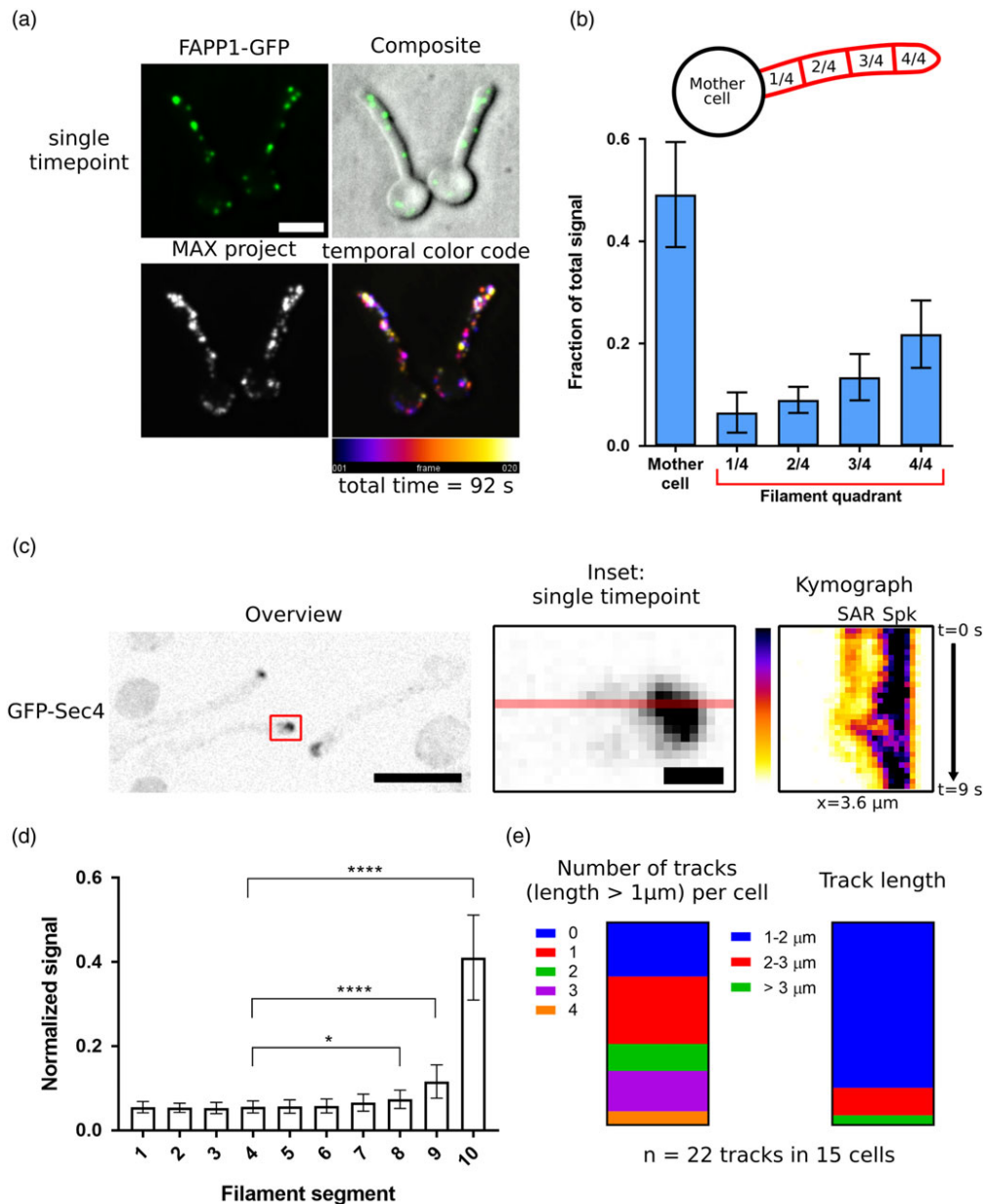
FIGURE 1 Golgi and secretory vesicles dynamics in *Candida albicans* filamentous cells. (a) Golgi marker FAPP1-GFP live cell Imaging. Twenty Z-stacks (31 sections each) were acquired (4.6 s per Z-stack) and sum projected for every time point. Max projection and temporal colour code are of all time points. Scale bar is 5 μm. (b) FAPP1-GFP distribution in the mother cell and filament quadrants (n = 13 cells). (c) Secretory vesicle marker GFP-Sec4 live cell imaging. Images were acquired at a single Z every 0.3 s. Scale bars are 10 μm (left) and 0.91 μm in inset (middle). Kymograph analysis of the area indicated in inset (right). (d) GFP-Sec4 distribution in 10 segments from the filament base (1) to the apex (10; n = 15 cells). (e) GFP-Sec4 tracking. Number of tracks longer than 1 μm per cell over 30 time points (total time 9 s; left) and track length distribution in all cells (n = 15 cells, 22 tracks)

along the cortex of the filamentous cell to distal transport along the core of the filament takes place (Cheung et al., 2008). Tracking of individual vesicles moving at least 1 μm along the hyphal length (Figure 1 e) showed that on average 1.5 ± 1.3 vesicle per time course move directionally towards the apex (n = 22), or ~10 vesicles per min. These vesicles move along short tracks, with more than 80% of tracks being 1–2 μm in length, and only one track being longer than 3 μm. Thus, directional movement of SV along the hyphal length appears to be limited to tracks not longer than ~10–20% of the total length of *C. albicans* hyphal filament.

The differential distribution of SVs is similar to that found in other polarised cells requiring the concentration of cargo and membrane at the growing hyphal tip, such as neurons and pollen tubes (Chebli et al., 2013; González & Couve, 2014), and in particular, other filamentous fungi that concentrate SVs in a Spk (Grove & Bracker, 1970; Riquelme, 2013; Riquelme & Sánchez-León, 2014). However, as we did not observe substantial directed movement, and as even directionally moving vesicles were limited to short tracks no longer than several microns, it appears that *C. albicans* SV dynamics do not conform to that of the above polarised cells, where SVs reach the

hyphal apex by travelling for many microns tethered to molecular motors moving along cytoskeletal tracks.

2.2 | Serial section transmission electron microscopy (ssTEM) reveals the cellular organisation of the hyphal filament tip

Following our identification of a distinct region of SV dynamics in the SAR, we further investigated this environment using ssTEM, providing the first high-resolution 3D view of *C. albicans* filamentous cell organisation (Figure 2a). ssTEM series acquired from both parallel (Figure 2b) and orthogonal (Figure 2c) angles compared with the long axis of the filamentous cell revealed the presence of vesicles with a spherical

appearance at the hyphal apex. Vesicles could be seen in multiple sequential sections (Figure 2d,e), suggesting they likely comprise the *C. albicans* Spk. Quantitative analysis (Figure 2f) revealed vesicles are 69.7 ± 10.8 nm in diameter (*n* = 10 cells, 720 vesicles), in close agreement with the 65 nm diameter vesicles induced by α-factor mating pheromone observed in *Saccharomyces cerevisiae* (Baba, Baba, Ohsumi, Kanaya, & Osumi, 1989). Within the Spk, vesicles are tightly packed, with more than 50% of vesicles in each Spk having a nearest neighbour distance (measured from one vesicle circumference to another) of less than 30 nm. The Spk also contains vesicles in proximity to the PM, with more than 25% of vesicles in each Spk found less than one vesicle diameter (i.e., 70 nm) away from the PM (Figure S1). We confirmed (Figure 2h) that the vesicles observed at the filamentous cell tip were indeed associated with the Spk, using immuno-gold
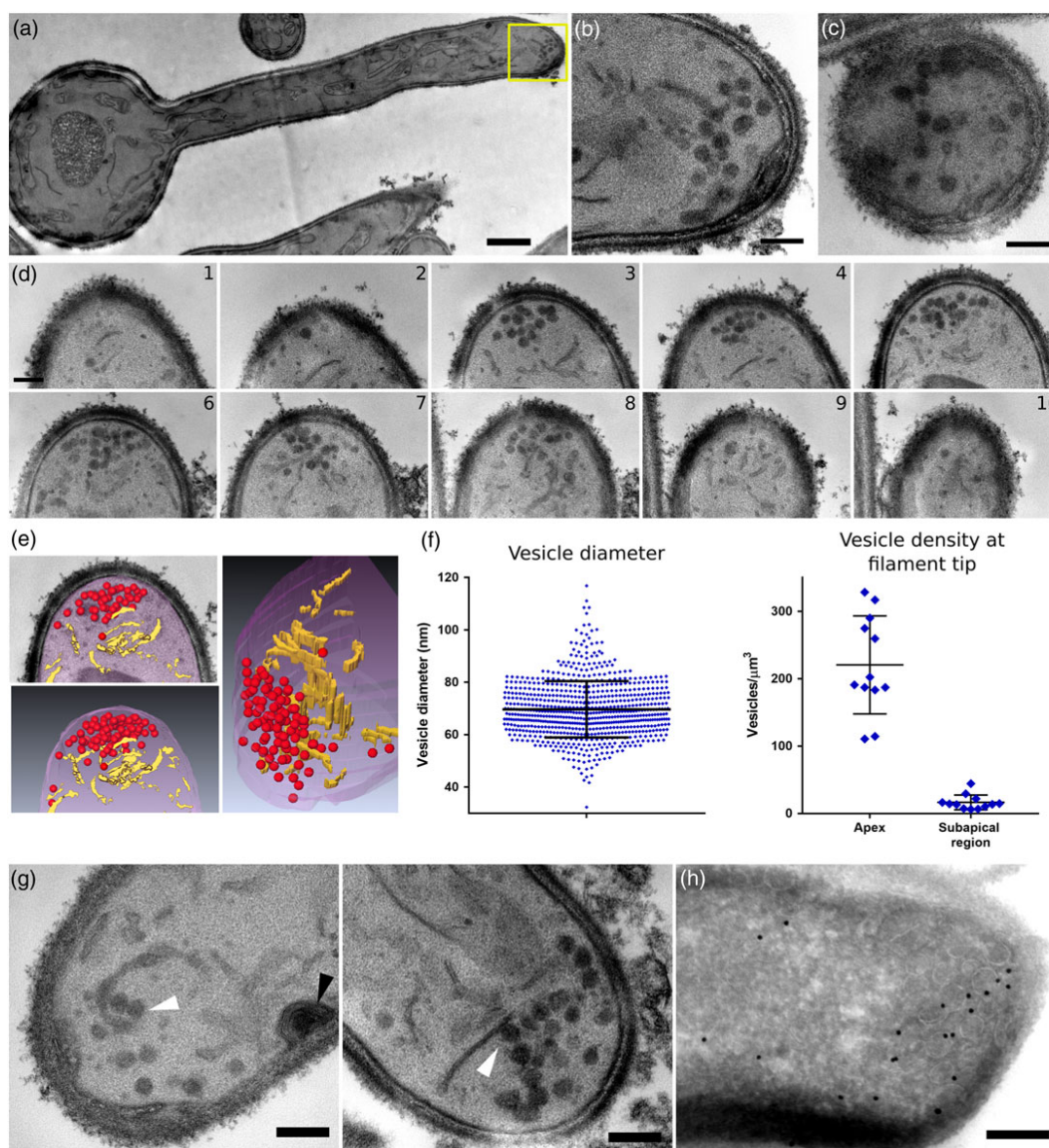
FIGURE 2 Cellular organisation of the filament tip by serial section transmission electron microscopy. Cells were serially imaged (section thickness 100 nm, up to 15 sections/cell) so that the entire hyphal tip could be examined. (a) Middle section from series acquired in parallel to the filament long axis. (b) Inset from panel (a). (c) Middle section from series acquired orthogonally to the filament long axis, vesicles appear circular in both (b) and (c). (d) Serial sections through the filament apex (10 sections, total thickness 1 μm). (e) Visualisation of the filament apex. Vesicles (red) and elongated membranes structures (yellow) are observed. (f) Quantification of vesicle diameter (*n* = 10 cells, 720 vesicles; left) and vesicle density (*n* = 12 cells, 879 vesicles; right) at the filament tip. (g) Membrane elements found in close proximity to vesicles, evoking budding events (white arrowheads). A site of endocytosis is also observed (black arrowhead). (h) Immuno-gold labelling of the Spk marker Mlc1-GFP. Scale bar is 1 μm in (a) and 200 nm in (b–d, g, and h)

labelling of cells expressing Mlc1-GFP, a Spk marker (Bartnicki-Garcia et al., 1995). Analysis of the number of vesicles found in different regions of the tip revealed that the apex (including the Spk) contains 57.8 ± 19.0 vesicles, whereas the SAR contains 15.5 ± 8.6 (*n* = 12 cells, 879 vesicles). Vesicle density calculations based on estimation of the volume of each region (Figure 2f) revealed a density of 220.4 ± 69.7 vesicles/μm^3 in the apex and 16.6 ± 10.5 vesicles/μm^3 in the SAR, a ratio of ~13 to 1. Vesicles outside of these regions were only sporadically observed. Surprisingly, vesicles in the Spk and the SARs were often in contact or proximity with elongated membranes structures, sometimes in a configuration evoking vesicle budding events (Figure 2g).

Comparative examination of a *sec3* deletion mutant, which has an increased number of vesicles at bud tips and a dramatic increase in Sec4 at the apex of germ tubes (Li et al., 2007), showed that there was a disorganisation of the Spk and that the swollen tips of *sec3* germ tubes contain vesicles concentrated in the middle of the tip and away from the PM (Figure 3).

2.3 | Estimation of the minimum rate of SV fusion with the PM

Next, we calculated the theoretical minimum rate of vesicle fusion with the apical PM required to sustain filamentous growth, based on cell geometry (Dataset S1). This rate was calculated to be 1.12 vesicles/s or 67 vesicles/min. Assuming an average vesicle number at the Spk of 60, the minimal Spk turnover time would be ~53 s, similar to previously published FRAP data (Jones & Sudbery, 2010). As the Spk appears to maintain its size throughout filamentous growth, we can assume that the minimal rate of vesicle influx into the Spk is identical to the calculated minimal rate of vesicle fusion. Thus, if the mechanism of vesicle delivery to the apex was based only on long-range vesicle trafficking, we would expect to observe 60–70 vesicles/min moving along the hyphal filament length towards the apex, whereas we only observed ~10 vesicles/min (Figure 1e),

suggesting short-range vesicle delivery significantly contributes to filamentous growth.

2.4 | The secretory pathway in *C. albicans* filamentous cells is organised in distinct structural domains

Our dynamic studies (Figure 1), together with modelling (Dataset S1), suggest that short-range SV delivery may have an important role in *C. albicans* filamentous growth. Furthermore, the presence of SVs found in close association with elongated membranes at the hyphal tip (Figure 2g) may be indicative of SV budding events. We hypothesised that these elongated membranes could be part of the ER or the Golgi, as these compartments were previously observed in *C. albicans* filamentous cells using fluorescent microscopy (Ghugtyal et al., 2015; Rida et al., 2006). Examination of the 3D membrane organisation in *C. albicans* hyphal filaments using ssTEM (Figure 4) in both short (Figure 4a,b) and longer filaments (Figure 4c–e) identified three distinct structural domains. First, emerging from the nuclear envelope into the nascent hyphal filament are sheet-like parallel membranes, spanning the majority of the length of the filamentous cell. Behind the hyphal apex, in a region roughly corresponding to the SAR, membrane parallelity is lost and shorter sheet-like membranes without an apparent orientation are observed. Such membrane organisation is similar to Golgi organisation in *S. cerevisiae*, where short membrane compartments apparently lacking orientation are found behind the emerging bud (Preuss, Mulholland, Franzusoff, Segev, & Botstein, 1992), and also resembles Golgi in other filamentous fungi (Pantazopoulou, 2016). It should be noted that there appears to be a continuous transition between these two membrane domains. Finally, at the apex, a Spk comprised of SVs is observed (see Figure 2). These three domains were observed in all filamentous cells examined and appear to be a hallmark of *C. albicans* hyphal endomembrane organisation.
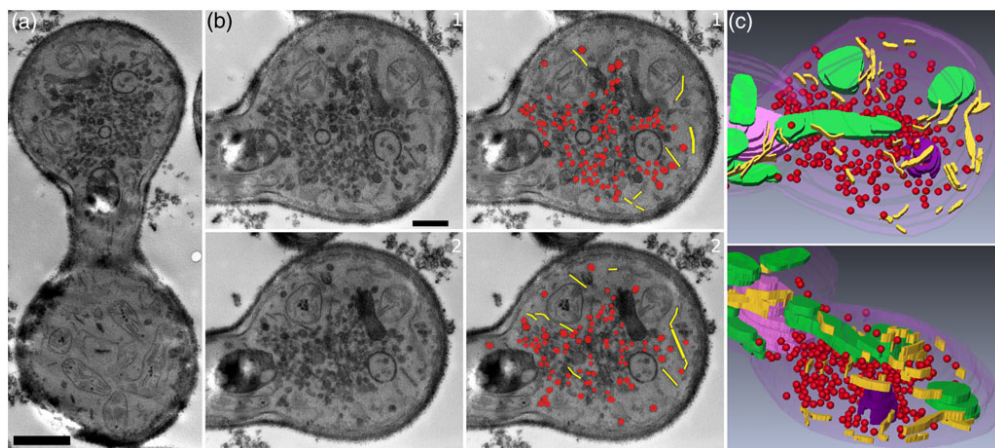
FIGURE 3 *sec3* mutant presents swollen tips with vesicles concentrated at the tip centre. *sec3* mutant cells were induced for 2 hr with serum, fixed and examined by serial section transmission electron microscopy. (a) Overview of filament organisation. (b) Two sections from the cell in panel (a), showing tip organisation. Elongated membranes and vesicles are highlighted in overlay. (c) Visualisation of three-dimensional features observed in (b) shown from different viewpoints. Colours represent: internal membranes (yellow), secretory vesicles (red), mitochondria (green), lipid droplets (pink), and autophagosome (purple). Scale bars are 1 μm in (a) and 500 nm in (b)
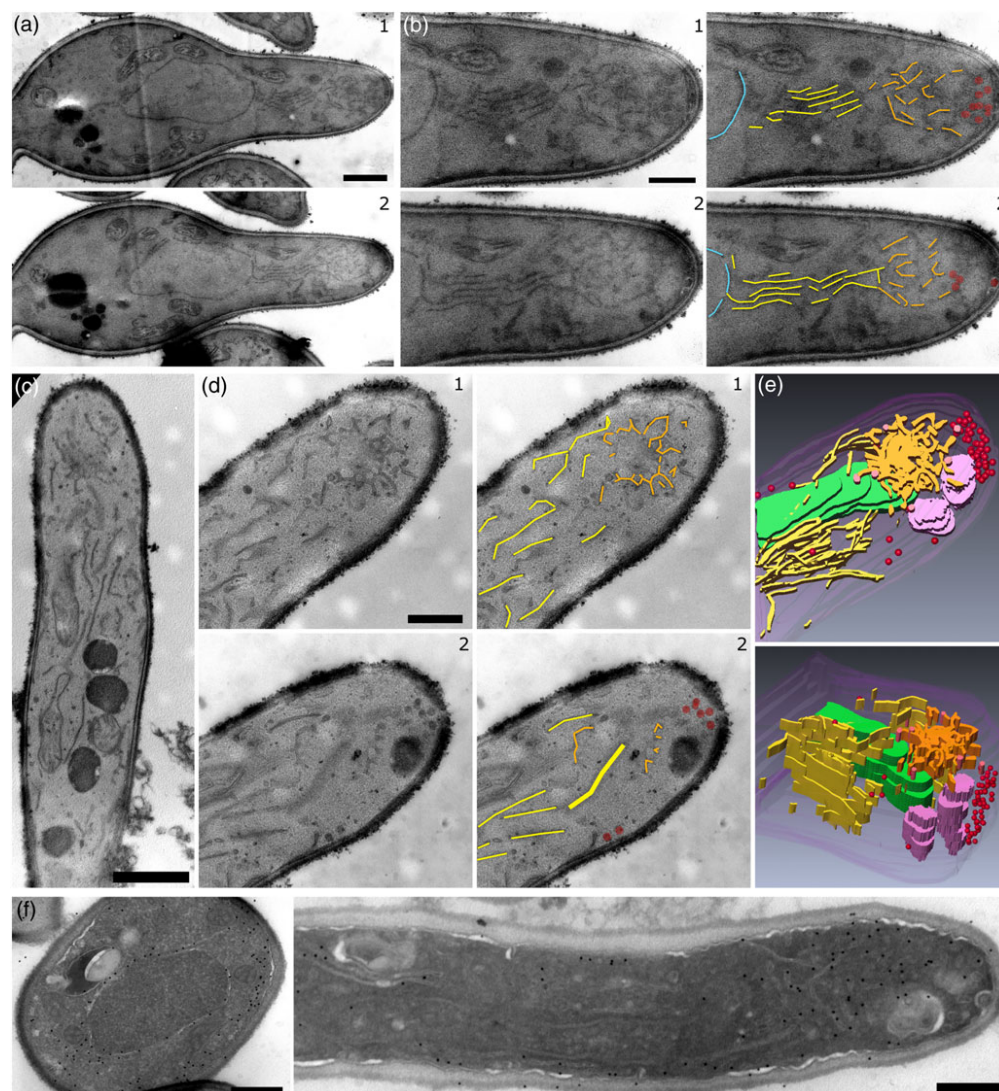
FIGURE 4 The secretory pathway in *Candida albicans* filaments is organised in distinct structural domains. (a) Serial section transmission electron microscopy of cells induced for 30 min. Two sections from a single series (1 and 2) are presented. (b) Detailed view of the filament in panel (a). Different membrane features are highlighted in overlay. (c) Cells induced for 60 min. Overview of filament organisation. (d) Detailed views of two sections of cell seen in panel (c). Different membrane features are highlighted in overlay. (e) Visualisation of three-dimensional features observed in all sections. Colours represent: nuclear envelope (light blue), parallel membranes (yellow), membranes oriented in various directions in the sub-apical region (orange), secretory vesicles (red), mitochondria (green), and lipid droplets (pink). (f) Immuno-gold labelling of the ER marker Sac1-GFP. Labelling of elongated membranes can be seen in mother cell (left) along the filament length and the sub-apical region (right). Scale bars are 1 μm in (a and c) and 500 nm in (b, d, and f)

To identify the compartments associated with these structural domains we performed immuno-gold labelling of cells expressing different markers. Sac1-GFP, which localises predominantly to the ER in *S. cerevisiae* (Faulhammer et al., 2005; Foti, Audhya, & Emr, 2001), was associated with parallel membranes spanning the filamentous cell length, as well as nonparallel membranes in the SAR (Figure 4f). As this lipid phosphatase has also been shown to cycle between the ER and Golgi (Faulhammer et al., 2005), the fenestrated Sac1 labelled structures near the apex could represent Golgi cisternae. Unfortunately, immuno-gold labelling of Golgi markers did not produce clear results, likely due to the nonstacked and dispersed organisation of this compartment in *C. albicans* (Rida et al., 2006). Upon disruption of actin cables, the Spk is no longer visible (Crampin et al., 2005) and, interestingly, treatment of cells with cytochalasin A (Akashi, Kanbe, & Tanaka, 1994) also disrupted the integrity of the

three organisational domains, suggesting a role for actin cables in their maintenance (Figure S2).

2.5 | Focused ion beam/scanning electron microscopy tomography (FIB/SEM) reveals distinct features in each structural domain

Using FIB/SEM, an emerging technique capable of producing large volume 3D ultrastructural datasets with high resolution in all axes (Heymann et al., 2006; Weiner et al., 2011; Weiner et al., 2016), we obtained a detailed 3D view of the hyphal filament organisation, including internal membranes, mitochondria, lipid droplets, sites of endocytosis, and SVs (Figure 5a; Movies S3 and S4). This analysis revealed several new features (Figure 5b). Along the hyphal filament
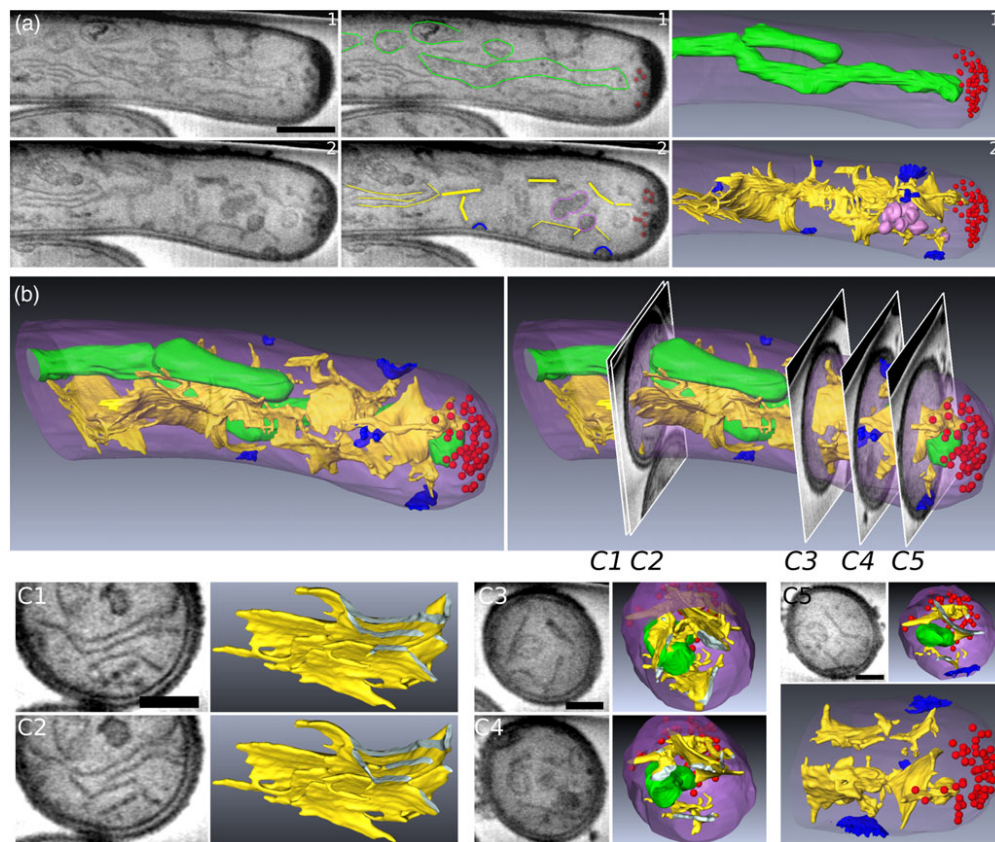
FIGURE 5 Focused ion beam/scanning electron microscopy tomography reveals distinct features in each structural domain of the *Candida albicans* filament. (a) Two sections from three-dimensional dataset are presented (left). Membrane features are highlighted in overlay (middle) and segmented in three dimensional from entire dataset (right). (b) Overview of filament organisation (left). Five sections with specific sites of interest are presented (right). (C1 and C2) Along the filament length curving membrane sheets connected through multiple helicoidal membrane motifs are observed. Different layer connectivity is observed in C1 versus C2. (C3 and C4) In the sub-apical region individual membrane sheets with tubular extensions are observed. (C5) Tubular extensions are found in direct contact with sites of endocytosis. Colours represent: internal membranes (yellow), secretory vesicles (red), mitochondria (green), lipid droplets (pink), and sites of endocytosis (blue). Scale bar in (a) is 1 μm and 500 nm in (C1, C3, and C5)

length, we observed that the parallel sheet-like membranes revealed by ssTEM are in fact a continuous structure composed of curving membrane sheets connected through multiple helicoidal membrane motifs (sheets connected by twisted membrane surfaces with helical edges of left- or right-handedness) sometimes referred to as "parking garage" structures, typical of ER organisation (Terasaki et al., 2013; Figure 5C1–2; Movie S5). The presence of this motif provides further evidence that the ER spans the majority of the hyphal filament length. In the SAR, we continued to observe the presence of membrane sheets, though these were found individually, were in a range of orientations (i.e., not in a parallel organisation) and were connected to many tubular extensions (Figure 5C3–4; Movie S6). Some of these extensions appeared to be in direct contact with sites of endocytosis, as well as extending into the apex where SVs were observed (in accordance with Figure 2; Figure 5C5; Movie S6). SVs were also occasionally observed within the SAR, though their lower density there, and the comparatively lower XY resolution of FIB/SEM compared with ssTEM, made it difficult to unambiguously identify them. Overall, membranes along the hyphal filament length and the SAR were overwhelmingly found in sheet and tubular organisation and were generally part of a continuous and widespread membrane network extending from the base of the hyphal filament all the way up to the

apex, where they were often in proximity to SVs within the Spk (Figure 2g). As SVs are seldom observed outside the apex and the SAR (and have limited directional movement), it stands to reason that membrane and cargo are delivered to the hyphal tip through the extended ER and Golgi network, followed by SV budding, thus requiring only short-range on-site SV trafficking towards the apical PM. Our calculation of the theoretical minimum rate of vesicle fusion with the apical PM required to sustain filamentous growth further supports the importance of short-range SV delivery.

Our work provides the first indication for an on-site SV delivery mechanism in *C. albicans*. We propose a model (Figure 6), in which the distance between the mother cell and the apex is traversed by the entire secretory apparatus moving up along the hyphal filament length, in the form of a network of interconnected ER and Golgi membranes organised in sheets and tubules. From this network, SVs bud either directly into the Spk, or in the SAR from which they are transported the short distance to the Spk, most likely along a network of actin cables that extended into the SAR (Sudbery, 2011). From the Spk, SVs are targeted to the exocyst complex and ultimately fuse with the PM (Jones & Sudbery, 2010). In this model, endocytic membranes entering through actin patches are incorporated into Golgi membranes at the SAR, and then later bud as SVs into the Spk, completing their
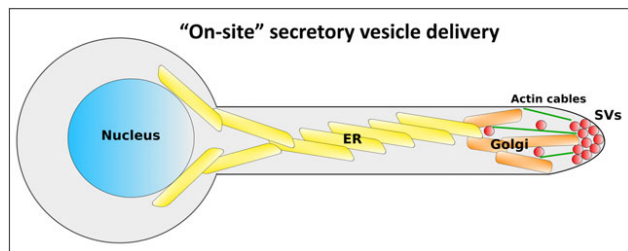
FIGURE 6 Model for secretory vesicle (SV) delivery to the *Candida albicans* filament tip. In this model, the ER and Golgi move into the extending filament allowing for on-site SV delivery requiring only short-range trafficking within the tip region. Nucleus (blue), ER (yellow), Golgi (orange), SVs (red), and actin cables (green) are presented

recycling (Ghugtyal et al., 2015). Indeed, endocytic recycling by way of the trans-Golgi network has recently been shown to be crucial for hyphal tip growth (Hernández-González et al., 2018).

Another implication of the proposed on-site SV delivery model is that the two main modes of *C. albicans* growth, budding and polarised growth, share common organisation principals, that is, orientation of the ER and Golgi towards the site of growth, on-site SV budding and short-range actin mediated trafficking of SV towards the PM, followed by fusion mediated by the exocyst. In budding growth, all the above steps are thought to occur in a highly constrained region at the site of the emerging bud (Ghugtyal et al., 2015; Mulholland et al., 1994; Preuss et al., 1991, 1992). In filamentous growth, the ER and Golgi extend far away towards the hyphal tip, but SV budding and delivery, also take place in a constrained region. The presence of a Spk during filamentous growth may simply reflect the higher flux of cargo and membrane required in this growth mode, compared with the small and transient SV accumulation during budding. The adoption of an on-site delivery mechanism by *C. albicans* could also be linked to the smaller size and slower extension rate of its hyphae compared with other filamentous fungi (Geitmann & Emons, 2000). The fact that *C. albicans* polarised growth is MT-independent (Rida et al., 2006) further emphasises the fundamental difference in its mechanism of SV delivery compared with other filamentous fungi relying on long-range SV deliver via MT tracks.

Our ultrastructural study of the *C. albicans* filamentous cell apex reveals a striking organisation of the Spk. The best described Spk thus far is found in *N. crassa*, where two populations of SV have been reported, a macro-vesicular population found in a ring like structure, thought to be conveyors of the β-1,3-glucan synthase complex, and a core made of micro-vesicles, containing chitin synthases (Richthammer et al., 2012; Riquelme et al., 2007; Sánchez-León et al., 2011; Verdín, Bartnicki-Garcia, & Riquelme, 2009). The observed MT converging or traversing the *N. crassa* Spk are thought to serve as tracks for SV delivery (Mouriño-Pérez, Roberson, & Bartnicki-García, 2006), together with actin cables also localised to the Spk (Berepiki, Lichius, Shoji, Tilsner, & Read, 2010). A similar Spk organisation with heterogenous SV populations has also been reported in *A. nidulans* and in other filamentous fungi, such as the plant pathogen *Pythium ultimum* and *Ascodesmis nigricans* (Grove & Bracker, 1970; Grove, Bracker, & Morre, 1970; Harris et al., 2005; Hohmann-Marriott et al., 2006). Overall, such studies, as well as

mathematical modelling and computer simulations, have led to the proposal that the Spk acts as a vesicle supply centre, whose purpose is to organise or direct SV traffic (Bartnicki-García, 2002; Bartnicki-Garcia, Hergert, & Gierz, 1989; Harris et al., 2005). In contrast, the *C. albicans* Spk is composed of a single population of 70 nm diameter vesicles, in close agreement with the SV diameter observed in *S. cerevisiae* (Baba et al., 1989), and close to the reported 70–90 nm diameter of the macrovesicles in the *A. nidulans* Spk (Harris et al., 2005). Thus, the *C. albicans* Spk structure is simpler than that in filamentous fungi such as *N. crassa* and *A. nidulans*, which may reflect its different biological function. In light of our proposed on-site vesicle delivery model, and the MT-independent SV trafficking in *C. albicans* (Rida et al., 2006), we find it highly unlikely that the *C. albicans* Spk serves as a MT-to-actin switching station. Instead, we propose it acts as a focal point for incoming SV traffic produced via budding in the SAR and apex region, and for outgoing traffic directed towards the PM. As Mlc1 and Bni1 are both found at the *C. albicans* Spk (Crampin et al., 2005; Martin, Walther, & Wendland, 2005; Rida et al., 2006), it is possible both inwards and outwards SV trafficking occur by movement along actin cables, though the precise function of the Spk in regulating these processes is still an open question. The proximity of SVs comprising the Spk with the apical PM (Figures 2 and S1) implies that outgoing SV trafficking occurs over a very short distance (less than 70 nm). We cannot, however, rule out the possibility that "early" SVs that might be pleomorphic, escape identification by electron microscopy. As a result, motor driven transport along actin cables may not be critical for this process, in contrast to previous models (Jones & Sudbery, 2010). Overall our results indicate that a fundamental distinction exists between the Spk of *C. albicans* and filamentous fungi, likely reflecting differences in their function during filamentous growth.

Our proposed "on-site" SV delivery during *C. albicans* filamentous growth represents a strong shift from previous models in filamentous fungi and resembles a recently discovered long-range delivery mechanism in neurons of the visual system of *Drosophila* (Shilo & Schejter, 2011). We speculate that this mechanism facilitates the local delivery to the hyphal tip of proteases, phospholipases, lipases, esterases, and peptide toxins, which together play important roles in the degradation of host tissue as well as cleavage of host immune defence proteins (da Silva Dantas et al., 2016; Schaller, Borelli, Korting, & Hube, 2005). As the endocytic collar is adjacent to the hypahl apex, local degradation and subsequent endocytosis may also facilitate nutrient acquisition during infection.

3 | EXPERIMENTAL PROCEDURES

3.1 | Growth conditions

Cells were grown at 30°C in yeast extract-peptone-dextrose (YEPD) medium. Serum induction was carried out as described previously (Bassilana, Blyth, & Arkowitz, 2003), using overnight cultures grown in YEPD that were back diluted in YEPD and grown for ~5 hr prior to the addition of 50% serum for 60 min unless indicated otherwise.

3.2 | Strains and plasmids

The prototrophic wild-type BWP17 strain (Wilson, Davis, & Mitchell, 1999) PY82 (*ura3Δ::λ imm434/ura3Δ::λ imm434 his1::hisG/HIS1:: his1::hisG arg4::hisG/URA3::ARG4::arg4::hisG*) (Bassilana et al., 2003) was used for EM analyses unless otherwise indicated. For Golgi analyses, strain PY2406 (BWP17 with *RP10::ARG4-pADH1-PH^{FAPP1[E50A,H54A]}-GFP*) was used (Ghugtyal et al., 2015). For SV analyses, strain PY3511 (BWP17 with *SEC4/SEC4::GFP-SEC4-URA3*) was generated by transformation of *pGFP-SEC4-utr* (Li et al., 2007) into BWP17. For ER immuno-EM analyses, strain PY1857 (BWP17 with *RP10::pADH1-GFP-SAC1*) was generated by transformation of pExpARG-*pADH1-GFP-SAC1* into BWP17.

3.3 | Cytochalasin A treatment

For cytochalasin A treatment, cells were serum induced for 30 min followed by treatment with 10 μM cytochalasin A (Molecular Probes) for 15 min. Cell were then fixed and examined by ssTEM.

3.4 | Light microscopy

Cells were imaged as described using a spinning-disc confocal microscopy (Ghugtyal et al., 2015) except that MetaMorph version 7.8.8.0 software (Molecular Devices) controlled the system and for GFP-Sec4 experiments a PLANAPO TIRF 100× TIRF × 1.45 NA objective was used. Z-stacks (0.4 μm each) were deconvolved with Huygens Professional software. For image analysis of Sec4 time courses, two-dimensional deconvolution was carried out with Huygens Professional software (version 18.04 Scientific-Volume Imaging) and SN of 10. Objects were identified for tracking using Volocity Software Version 6.3 (PerkinElmer) as previously described using the SD mode (Ghugtyal et al., 2015), where the selection is based on SDs above the mean intensity. Live imaging of GFP-Sec4 was performed in growing filaments of 15 different cells over 9 s, imaging a single focal plane with 300 ms exposure time. Quantitative analysis was used to determine the relative Sec4-GFP signal intensities along the hyphal filament (Figure 1d). Filaments of average length 10 μm were divided into 10 segments, with the total intensity measured in each segment over the time course of the imaging.

3.5 | Serial section transmission electron microscopy

C. albicans cells were induced for filamentous growth, after which samples were fixed and stained using potassium permanganate, previously shown to provide excellent membrane contrast in yeast (Wright, 2000). Samples were prepared according to (Wright, 2000). Cell pellets were fixed in a 1.6% glutataraldehyde solution in 0.1 M sodium phosphate buffer (pH 7.4) at room temperature and stored overnight at 4°C. After three rinsing in DDW (15 min each), pellets were postfixed in a freshly prepared 2% potassium permanganate (KMnO$_4$) solution in DDW for 2 hr (Wright, 2000). KMnO$_4$ baths were changed every 30 min. Cells were subsequently rinsed in DDW (five times, 15 min each) and dehydrated in a series of acetone baths (90%,

100% three times, 15 min each) and progressively embedded in Epon 812 (Fluka) resin (acetone/resin 1:1, 100% resin two times, 2 hr for each bath). Resin blocs were finally left to harden at 60°C in an oven for 2 days. Ultrathin serial sections (100 nm) were obtained with a Reichert Ultracut S ultra-microtome equipped with a Drukker International diamond knife and collected on copper slot grids with a formvar support film. TEM observations were performed with a JEOL JEM-1400 transmission electron microscope, equipped with a Morada camera, at a 100 kV acceleration voltage. Overall, 18 hyphal filaments were imaged by ssTEM, 12 wild-type cells serum induced for 60 min, two wild-type cells serum induced for 30 min, two wild-type cells treated with cytochalasin A, and two *sec3* mutant cells serum induced for 120 min. Up to 15 serial sections (100 nm thickness) of each individual hyphal apex were imaged.

3.6 | Focused ion beam/scanning electron microscopy tomography

Samples for FIB/SEM tomography were prepared the same way as for ssTEM. Data were acquired using a Helios-600 Dual Beam of FEI, Thermo Fisher, USA, as described earlier in (Weiner et al., 2011) at the Weizmann Institute of Science, Rehovot, Israel. The large frontal trench was milled with an Ion beam of 30 kV, 20 nA, and the serial slicing was performed with a 30 kV, 460pA beam. To reduce the charging artefacts SEM images low energy secondary electrons were filtered by applying a negative voltage of −22 V on the suction tube electrode. XY pixel size was 6.4 or 7 nm and slice thickness 10 nm. Data were collected in two independent runs, providing views of six hyphal filaments. For segmentation and analysis around 150 sections traversing a single filamentous cell width were used. Two filamentous cells were segmented in their entirety.

3.7 | Immuno-gold labelling

Immuno-gold staining was done according to (Griffith, Mari, De Mazière, & Reggiori, 2008). Cells were mixed with an equal volume of double-strength fixative [4% paraformaldehyde (PFA) 0.4% glutaraldehyde (GA) in 0.1 M PHEM buffer (20 mM PIPES, 50 mM HEPES, pH 6.9, 20 mM EGTA, 4 mM MgCl$_2$)] and incubated for 20 min at room temperature on a roller. Then, the fixative was replaced by fresh one at the concentration of 2% PFA, 0.2% GA in PHEM for additional 3 hr and were processed for ultra-cryomicrotomy according to a slightly modified Tokuyasu method for yeast. In brief, after rinsing in PHEM buffer and incubation in 1% periodic acid in PHEM buffer for 1 hr, three times washed cell suspension was spun down in 12% gelatin in PHEM. After immersion in 2.3 M sucrose overnight at 4°C, the samples were rapidly frozen in liquid nitrogen. Ultrathin (70 nm thick) cryo-sections were prepared with an ultra-cryomicrotome (Leica EMFCS, Austria) and mounted on formvar-coated nickel grids (Electron Microscopy Sciences, Fort Washington, PA, USA). Immuno-staining was processed with an automated immuno-gold labelling system Leica EM IGL as following: the grids were incubated successively in PBS containing 50 mM NH4Cl (two times, 5 min), PBS containing 1% BSA (two times, 5 min.), PBS containing the relevant

primary antibody in 1% BSA for 1 hr, PBS containing 0.1% BSA (three times, 5 min), PBS containing 1% BSA and 15 nm colloidal gold conjugated protein A (CMC, University Medical Center, Utrecht, The Netherlands), PBS containing 0.1% BSA for 5 min, PBS for 5 min twice. Lastly, the samples were fixed for 10 min with 1% glutaraldehyde, rinsed in distilled water and were contrasted with a mixture of methylcellulose and 0.3% uranyl acetate on ice. After having been dried in air, sections were examined under a JEOL 1400 transmission electron microscope.

3.8 | Image analysis and data quantification

Data were analysed and quantified using Fiji (https://fiji.sc/) for light microscopy and ssTEM diameter measurement. Amira (Thermo Fisher Scientific—FEI) was used for ssTEM and FIB/SEM tomography data alignment, manual segmentation and analysis. The difference between Sec4 intensities along the filament length was evaluated using unpaired t test between Segments 4 and 8, 4 and 9, and 4 and 10. $P < 0.05$ was considered as significant: $*P < 0.05$, $**P < 0.01$, $***P < 0.001$, and $****P < 0.0001$. ssTEM quantification: for vesicle diameter measurement, each vesicle was manually segmented using Fiji. For the number of vesicles measurement, the apex was defined as the region extending between 0 and 500 nm from the tip, and the SAR was defined as the area extending between 500 and 1,500 nm from the tip. For density calculation the apex was modelled as a half-sphere with radius 500 nm, and the SAR as a cylinder with length 1,000 nm and a diameter measured from the middle section of each cell. For nearest neighbour distance calculations, the distance from each vesicle circumference to the circumference of its nearest neighbour was measured ($n = 6$ cells, 503 vesicle pairs). Negative values represent perceived vesicle overlap due to the TEM image being a projection of a 100 nm thick section that may contain two vesicles aligned in the Z-axis. For distance to the PM calculation, the PM was outlined using Fiji, and the distance between each vesicle and the nearest PM segment was measured ($n = 6$ cells, 489 vesicles). FIB/SEM tomography data were aligned using Amira and bandpass filtered using Fiji. Data were manually segmented using Amira. Virtual slices oriented along the long axis of the hyphal filament are presented in Figure 5a. All quantitative data in the manuscript are presented as mean, with error bars presented as SD.

ORCID

Robert A. Arkowitz http://orcid.org/0000-0002-5216-5013

REFERENCES

Akashi, T., Kanbe, T., & Tanaka, K. (1994). The role of the cytoskeleton in the polarized growth of the germ tube in *Candida albicans*. *Microbiology*, *140*, 271–280. https://doi.org/10.1099/13500872-140-2-271

Anderson, J. M., & Soll, D. R. (1986). Differences in actin localization during bud and hypha formation in the yeast *Candida albicans*. *Microbiology*, *132*, 2035–2047. https://doi.org/10.1099/00221287-132-7-2035

Baba, M., Baba, N., Ohsumi, Y., Kanaya, K., & Osumi, M. (1989). Three-dimensional analysis of morphogenesis induced by mating pheromone alpha factor in *Saccharomyces cerevisiae*. *Journal of Cell Science*, *94*.

Bartnicki-García S. (2002). *Hyphal tip growth: Outstanding questions. "Molecular biology of fungal development"* (H. D. Osiewacz) Marcel Dekker: New York.

Bartnicki-Garcia, S., Bartnicki, D. D., Gierz, G., López-Franco, R., & Bracker, C. E. (1995). Evidence that Spitzenkörper behavior determines the shape of a fungal hypha: A test of the hyphoid model. *Experimental Mycology*, *19*, 153–159. https://doi.org/10.1006/emyc.1995.1017

Bartnicki-Garcia, S., Hergert, F., & Gierz, G. (1989). Computer simulation of fungal morphogenesis and the mathematical basis for hyphal (tip) growth. *Protoplasma*, *153*, 46–57. https://doi.org/10.1007/BF01322464

Bar-Yosef, H., Gildor, T., Ramírez-Zavala, B., Schmauch, C., Weissman, Z., Pinsky, M., ... Kornitzer, D. (2018). A global analysis of kinase function in *Candida albicans* hyphal morphogenesis reveals a role for the endocytosis regulator Akl1. *Frontiers in Cellular and Infection Microbiology*, *8*, 17. https://doi.org/10.3389/fcimb.2018.00017

Bassilana, M., Blyth, J., & Arkowitz, R. A. (2003). Cdc24, the GDP-GTP exchange factor for Cdc42, is required for invasive hyphal growth of *Candida albicans*. *Eukaryotic Cell*, *2*, 9–18. https://doi.org/10.1128/EC.2.1.9-18.2003

Berepiki, A., Lichius, A., & Read, N. D. (2011). Actin organization and dynamics in filamentous fungi. *Nature Reviews. Microbiology*, *9*, 876–887. https://doi.org/10.1038/nrmicro2666

Berepiki, A., Lichius, A., Shoji, J.-Y., Tilsner, J., & Read, N. D. (2010). F-actin dynamics in *Neurospora crassa*. *Eukaryotic Cell*, *9*, 547–557. https://doi.org/10.1128/EC.00253-09

Bishop, A., Lane, R., Beniston, R., Chapa-y-Lazo, B., Smythe, C., & Sudbery, P. (2010). Hyphal growth in *Candida albicans* requires the phosphorylation of Sec2 by the Cdc28-Ccn1/Hgc1 kinase. *The EMBO Journal*, *29*, 2930–2942. https://doi.org/10.1038/emboj.2010.158

Caballero-Lima, D., Kaneva, I. N., Watton, S. P., Sudbery, P. E., & Craven, C. J. (2013). The spatial distribution of the exocyst and actin cortical patches is sufficient to organize hyphal tip growth. *Eukaryotic Cell*, *12*, 998–1008. https://doi.org/10.1128/EC.00085-13

Chebli, Y., Kroeger, J., & Geitmann, A. (2013). Transport logistics in pollen tubes. *Molecular Plant*, *6*, 1037–1052. https://doi.org/10.1093/mp/sst073

Cheung, A. Y., Duan, Q., Costa, S. S., de Graaf, B. H. J., SDi Stilio, V. S., Feijo, J., & Wu, H.-M. (2008). The dynamic pollen tube cytoskeleton: Live cell studies using actin-binding and microtubule-binding reporter proteins. *Molecular Plant*, *1*, 686–702. https://doi.org/10.1093/mp/ssn026

Crampin, H., Finley, K., Gerami-Nejad, M., Court, H., Gale, C., Berman, J., & Sudbery, P. (2005). *Candida albicans* hyphae have a Spitzenkörper that is distinct from the polarisome found in yeast and pseudohyphae. *Journal of Cell Science*, *118*, 2935–2947. https://doi.org/10.1242/jcs.02414

da Silva Dantas, A., Lee, K. K., Raziunaite, I., Schaefer, K., Wagener, J., Yadav, B., & Gow, N. A. (2016). Cell biology of *Candida albicans*-host interactions. *Current Opinion in Microbiology*, *34*, 111–118. https://doi.org/10.1016/j.mib.2016.08.006

Dalle, F., Wächtler, B., L'Ollivier, C., Holland, G., Bannert, N., Wilson, D., ... Hube, B. (2010). Cellular interactions of *Candida albicans* with human oral epithelial cells and enterocytes. *Cellular Microbiology*, *12*, 248–271. https://doi.org/10.1111/j.1462-5822.2009.01394.x

Faulhammer, F., Konrad, G., Brankatschk, B., Tahirovic, S., Knödler, A., & Mayinger, P. (2005). Cell growth-dependent coordination of lipid signaling and glycosylation is mediated by interactions between Sac1p and Dpm1p. *The Journal of Cell Biology*, *168*, 185–191. https://doi.org/10.1083/jcb.200407118

Foti, M., Audhya, A., & Emr, S. D. (2001). Sac1 lipid phosphatase and Stt4 phosphatidylinositol 4-kinase regulate a pool of phosphatidylinositol 4-phosphate that functions in the control of the actin cytoskeleton and vacuole morphology. *Molecular Biology of the Cell*, *12*, 2396–2411. https://doi.org/10.1091/mbc.12.8.2396

Geitmann, A., & Emons, A. M. (2000). The cytoskeleton in plant and fungal cell tip growth. *Journal of Microscopy*, *198*, 218–245. https://doi.org/10.1046/j.1365-2818.2000.00702.x

Ghugtyal, V., Garcia-Rodas, R., Seminara, A., Schaub, S., Bassilana, M., & Arkowitz, R. A. (2015). Phosphatidylinositol-4-phosphate-dependent membrane traffic is critical for fungal filamentous growth. *Proceedings of the National Academy of Sciences*, *112*, 8644–8649. https://doi.org/10.1073/pnas.1504259112

González, C., & Couve, A. (2014). The axonal endoplasmic reticulum and protein trafficking: Cellular bootlegging south of the soma. *Seminars in Cell & Developmental Biology*, *27*, 23–31. https://doi.org/10.1016/j.semcdb.2013.12.004

Gow, N. A., & Hube, B. (2012). Importance of the *Candida albicans* cell wall during commensalism and infection. *Current Opinion in Microbiology*, *15*, 406–412. https://doi.org/10.1016/j.mib.2012.04.005

Griffith, J., Mari, M., De Mazière, A., & Reggiori, F. (2008). A cryosectioning procedure for the ultrastructural analysis and the immunogold labelling of yeast *Saccharomyces cerevisiae*. *Traffic*, *9*, 1060–1072. https://doi.org/10.1111/j.1600-0854.2008.00753.x

Grove, S. N., & Bracker, C. E. (1970). Protoplasmic organization of hyphal tips among fungi: Vesicles and Spitzenkörper. *Journal of Bacteriology*, *104*, 989–1009.

Grove, S. N., Bracker, C. E., & Morre, D. J. (1970). An ultrastructural basis for hyphal tip growth in *Pythium ultimum*. *American Journal of Botany*, *57*, 245–266. https://doi.org/10.1002/j.1537-2197.1970.tb09814.x

Guo, P. P., Yong, J. Y. A., Wang, Y. M., & Li, C. R. (2016). Sec15 links bud site selection to polarised cell growth and exocytosis in *Candida albicans*. *Scientific Reports*, *6*, 26464. https://doi.org/10.1038/srep26464

Hall, R. A., & Gow, N. A. R. (2013). Mannosylation in *Candida albicans*: Role in cell wall function and immune recognition. *Molecular Microbiology*, *90*, 1147–1161. https://doi.org/10.1111/mmi.12426

Harris, S. D. (2013). Golgi organization and the apical extension of fungal hyphae: An essential relationship. *Molecular Microbiology*, *89*, 212–215. https://doi.org/10.1111/mmi.12291

Harris, S. D., Read, N. D., Roberson, R. W., Shaw, B., Seiler, S., Plamann, M., & Momany, M. (2005). Polarisome meets spitzenkörper: Microscopy, genetics. *And Genomics Converge. Eukaryot Cell*, *4*, 225–229. https://doi.org/10.1128/EC.4.2.225-229.2005

Hernández-González, M., Bravo-Plaza, I., Pinar, M., de los Ríos, V., Arst, H. N., & Peñalva, M. A. (2018). Endocytic recycling via the TGN underlies the polarized hyphal mode of life. *PLoS Genetics*, *14*. e1007291

Heymann, J. A. W., Hayles, M., Gestmann, I., Giannuzzi, L. A., Lich, B., & Subramaniam, S. (2006). Site-specific 3D imaging of cells and tissues with a dual beam microscope. *Journal of Structural Biology*, *155*, 63–73. https://doi.org/10.1016/j.jsb.2006.03.006

Höfs, S., Mogavero, S., & Hube, B. (2016). Interaction of *Candida albicans* with host cells: Virulence factors, host defense, escape strategies. *And the Microbiota. J Microbiol*, *54*, 149–169. https://doi.org/10.1007/s12275-016-5514-0

Hohmann-Marriott, M. F., Uchida, M., van de Meene, A. M. L., Garret, M., Hjelm, B. E., Kokoori, S., & Roberson, R. W. (2006). Application of electron tomography to fungal ultrastructure studies. *The New Phytologist*, *172*, 208–220. https://doi.org/10.1111/j.1469-8137.2006.01868.x

Jones, L. A., & Sudbery, P. E. (2010). Spitzenkorper, exocyst, and polarisome components in *Candida albicans* hyphae show different patterns of localization and have distinct dynamic properties. *Eukaryotic Cell*, *9*, 1455–1465. https://doi.org/10.1128/EC.00109-10

Labbaoui, H., Bogliolo, S., Ghugtyal, V., Solis, N. V., Filler, S. G., Arkowitz, R. A., & Bassilana, M. (2017). Role of Arf GTPases in fungal morphogenesis and virulence. *PLoS Pathogens*, *13*, e1006205. https://doi.org/10.1371/journal.ppat.1006205

Lewis, L. E., Bain, J. M., Lowes, C., Gillespie, C., Rudkin, F. M., Gow, N. A. R., & Erwig, L.-P. (2012). Stage specific assessment of *Candida albicans* phagocytosis by macrophages identifies cell wall composition and morphogenesis as key determinants. *PLoS Pathogens*, *8*, e1002578. https://doi.org/10.1371/journal.ppat.1002578

Li, C.-R., Lee, R. T.-H., Wang, Y.-M., Zheng, X.-D., & Wang, Y. (2007). Candida albicans hyphal morphogenesis occurs in Sec3p-independent and Sec3p-dependent phases separated by septin ring formation. *Journal of Cell Science*, *120*, 1898–1907. https://doi.org/10.1242/jcs.002931

Mao, Y., Kalb, V. F., & Wong, B. (1999). Overexpression of a dominant-negative allele of *SEC4* inhibits growth and protein secretion in *Candida albicans*. *Journal of Bacteriology*, *181*, 7235.

Martin, R., Hellwig, D., Schaub, Y., Bauer, J., Walther, A., & Wendland, J. (2007). Functional analysis of *Candida albicans* genes whose *Saccharomyces cerevisiae* homologues are involved in endocytosis. *Yeast*, *24*, 511–522. https://doi.org/10.1002/yea.1489

Martin, R., Walther, A., & Wendland, J. (2005). Ras1-induced hyphal development in *Candida albicans* requires the formin Bni1. *Eukaryotic Cell*, *4*, 1712–1724. https://doi.org/10.1128/EC.4.10.1712-1724.2005

Mouriño-Pérez, R. R., Riquelme, M., Callejas-Negrete, O. A., & Galván-Mendoza, J. I. (2016). Microtubules and associated molecular motors in *Neurospora crassa*. *Mycologia*, *108*, 515–527. https://doi.org/10.3852/15-323

Mouriño-Pérez, R. R., Roberson, R. W., & Bartnicki-García, S. (2006). Microtubule dynamics and organization during hyphal growth and branching in *Neurospora crassa*. *Fungal Genetics and Biology*, *43*, 389–400. https://doi.org/10.1016/j.fgb.2005.10.007

Moyes, D. L., Richardson, J. P., & Naglik, J. R. (2015). *Candida albicans*-epithelial interactions and pathogenicity mechanisms: Scratching the surface. *Virulence*, *6*, 338–346. https://doi.org/10.1080/21505594.2015.1012981

Moyes, D. L., Wilson, D., Richardson, J. P., Mogavero, S., Tang, S. X., Wernecke, J., ... Naglik, J. R. (2016). Candidalysin is a fungal peptide toxin critical for mucosal infection. *Nature*, *532*, 64–68. https://doi.org/10.1038/nature17625

Mulholland, J., Preuss, D., Moon, A., Wong, A., Drubin, D., & Botstein, D. (1994). Ultrastructure of the yeast actin cytoskeleton and its association with the plasma membrane. *The Journal of Cell Biology*, *125*, 381–391. https://doi.org/10.1083/jcb.125.2.381

Naglik, J. R., König, A., Hube, B., & Gaffen, S. L. (2017). *Candida albicans*-epithelial interactions and induction of mucosal innate immunity. *Current Opinion in Microbiology*, *40*, 104–112. https://doi.org/10.1016/j.mib.2017.10.030

Pantazopoulou, A. (2016). The Golgi apparatus: Insights from filamentous fungi. *Mycologia*, *108*, 603–622. https://doi.org/10.3852/15-309

Pantazopoulou, A., Pinar, M., Xiang, X., & Peñalva, M. A. (2014). Maturation of late Golgi cisternae into RabE (RAB11) exocytic post-Golgi carriers visualized in vivo. *Molecular Biology of the Cell*, *25*, 2428–2443. https://doi.org/10.1091/mbc.e14-02-0710

Peñalva, M. A., Zhang, J., Xiang, X., & Pantazopoulou, A. (2017). Transport of fungal RAB11 secretory vesicles involves myosin-5, dynein/dynactin/p25, and kinesin-1 and is independent of kinesin-3. *Molecular Biology of the Cell*, *28*, 947–961. https://doi.org/10.1091/mbc.e16-08-0566

Pericolini, E., Perito, S., Castagnoli, A., Gabrielli, E., Mencacci, A., Blasi, E., ... Wheeler, R. T. (2018). Epitope unmasking in vulvovaginal candidiasis is associated with hyphal growth and neutrophilic infiltration. *PLoS One*, *13*, e0201436. https://doi.org/10.1371/journal.pone.0201436

Pfaller, M. A., & Diekema, D. J. (2010). Epidemiology of invasive mycoses in North America. *Critical Reviews in Microbiology*, *36*, 1–53. https://doi.org/10.3109/10408410903241444

Phan, Q. T., Myers, C. L., Fu, Y., Sheppard, D. C., Yeaman, M. R., Welch, W. H., ... Filler, S. G. (2007). Als3 is a *Candida albicans* invasin that binds to cadherins and induces endocytosis by host cells. *PLoS Biology*, *5*, e64. https://doi.org/10.1371/journal.pbio.0050064

Preuss, D., Mulholland, J., Franzusoff, A., Segev, N., & Botstein, D. (1992). Characterization of the *Saccharomyces* Golgi complex through the cell cycle by immunoelectron microscopy. *Molecular Biology of the Cell*, *3*, 789–803. https://doi.org/10.1091/mbc.3.7.789

Preuss, D., Mulholland, J., Kaiser, C. A., Orlean, P., Albright, C., Rose, M. D., ... Botstein, D. (1991). Structure of the yeast endoplasmic reticulum: Localization of ER proteins using immunofluorescence and immunoelectron microscopy. *Yeast*, *7*, 891–911. https://doi.org/10.1002/yea.320070902

Richthammer, C., Enseleit, M., Sanchez-Leon, E., März, S., Heilig, Y., Riquelme, M., & Seiler, S. (2012). *RHO1* and *RHO2* share partially overlapping functions in the regulation of cell wall integrity and hyphal polarity in *Neurospora crassa*. *Molecular Microbiology*, *85*, 716–733. https://doi.org/10.1111/j.1365-2958.2012.08133.x

Rida, P. C. G., Nishikawa, A., Won, G. Y., & Dean, N. (2006). Yeast-to-hyphal transition triggers formin-dependent Golgi localization to the growing tip in *Candida albicans*. *Molecular Biology of the Cell*, *17*, 4364–4378. https://doi.org/10.1091/mbc.e06-02-0143

Riquelme, M. (2013). Tip growth in filamentous fungi: A road trip to the apex. *Annual Review of Microbiology*, *67*, 587–609. https://doi.org/10.1146/annurev-micro-092412-155652

Riquelme, M., Bartnicki-García, S., González-Prieto, J. M., Sánchez-León, E., Verdín-Ramos, J. A., Beltrán-Aguilar, A., & Freitag, M. (2007). Spitzenkorper localization and intracellular traffic of green fluorescent protein-labeled CHS-3 and CHS-6 chitin synthases in living hyphae of *Neurospora crassa*. *Eukaryotic Cell*, *6*, 1853–1864. https://doi.org/10.1128/EC.00088-07

Riquelme, M., & Sánchez-León, E. (2014). The Spitzenkörper: A choreographer of fungal growth and morphogenesis. *Current Opinion in Microbiology*, *20*, 27–33. https://doi.org/10.1016/j.mib.2014.04.003

Sánchez-León, E., Verdín, J., Freitag, M., Roberson, R. W., Bartnicki-Garcia, S., & Riquelme, M. (2011). Traffic of chitin synthase 1 (CHS-1) to the Spitzenkörper and developing septa in hyphae of *Neurospora crassa*: Actin dependence and evidence of distinct microvesicle populations. *Eukaryotic Cell*, *10*, 683–695. https://doi.org/10.1128/EC.00280-10

Schaller, M., Borelli, C., Korting, H. C., & Hube, B. (2005). Hydrolytic enzymes as virulence factors of *Candida albicans*. *Mycoses*, *48*, 365–377. https://doi.org/10.1111/j.1439-0507.2005.01165.x

Shilo, B.-Z., & Schejter, E. D. (2011). Regulation of developmental intercellular signalling by intracellular trafficking. *The EMBO Journal*, *30*, 3516–3526. https://doi.org/10.1038/emboj.2011.269

Sudbery, P. E. (2011). Growth of *Candida albicans* hyphae. *Nature Reviews. Microbiology*, *9*, 737–748. https://doi.org/10.1038/nrmicro2636

Terasaki, M., Shemesh, T., Kasthuri, N., Klemm, R. W., Schalek, R., Hayworth, K. J., ... Kozlov, M. M. (2013). Stacked endoplasmic reticulum sheets are connected by helicoidal membrane motifs. *Cell*, *154*, 285–296. https://doi.org/10.1016/j.cell.2013.06.031

Verdín, J., Bartnicki-Garcia, S., & Riquelme, M. (2009). Functional stratification of the Spitzenkörper of Neurospora crassa. *Molecular Microbiology*, *74*, 1044–1053. https://doi.org/10.1111/j.1365-2958.2009.06917.x

Wakade, R., Labbaoui, H., Stalder, D., Arkowitz, R. A., & Bassilana, M. (2017). Overexpression of *YPT6* restores invasive filamentous growth and secretory vesicle clustering in a *Candida albicans arl1* mutant. *Small GTPases*, 1–7. https://doi.org/10.1080/21541248.2017.1378157

Weiner, A., Dahan-Pasternak, N., Shimoni, E., Shinder, V., von Huth, P., Elbaum, M., & Dzikowski, R. (2011). 3D nuclear architecture reveals coupled cell cycle dynamics of chromatin and nuclear pores in the malaria parasite *Plasmodium falciparum*. *Cellular Microbiology*, *13*, 967–977. https://doi.org/10.1111/j.1462-5822.2011.01592.x

Weiner, A., Mellouk, N., Lopez-Montero, N., Chang, Y.-Y., Souque, C., Schmitt, C., & Enninga, J. (2016). Macropinosomes are key players in early *Shigella* invasion and vacuolar escape in epithelial cells. *PLoS Pathogens*, *12*, e1005602. https://doi.org/10.1371/journal.ppat.1005602

Wheeler, R. T., Kombe, D., Agarwala, S. D., & Fink, G. R. (2008). Dynamic, morphotype-specific *Candida albicans* β-glucan exposure during infection and drug treatment. *PLoS Pathogens*, *4*, e1000227. https://doi.org/10.1371/journal.ppat.1000227

Wilson, R. B., Davis, D., & Mitchell, A. P. (1999). Rapid hypothesis testing with *Candida albicans* through gene disruption with short homology regions. *Journal of Bacteriology*, *181*, 1868–1874.

Wright, R. (2000). Transmission electron microscopy of yeast. *Microscopy Research and Technique*, *51*, 496–510. https://doi.org/10.1002/1097-0029(20001215)51:6<496::AID-JEMT2>3.0.CO;2-9

Yogev, S., Schejter, E. D., & Shilo, B.-Z. (2010). Polarized secretion of *Drosophila* EGFR ligand from photoreceptor neurons is controlled by ER localization of the ligand-processing machinery. *PLoS Biology*, *8*, e1000505. https://doi.org/10.1371/journal.pbio.1000505

Zeng, G., Wang, Y.-M., & Wang, Y. (2012). Cdc28-Cln3 phosphorylation of Sla1 regulates actin patch dynamics in different modes of fungal growth. *Molecular Biology of the Cell*, *23*, 3485–3497. https://doi.org/10.1091/mbc.e12-03-0231

SUPPORTING INFORMATION

Additional supporting information may be found online in the Supporting Information section at the end of the article.

Dataset S1
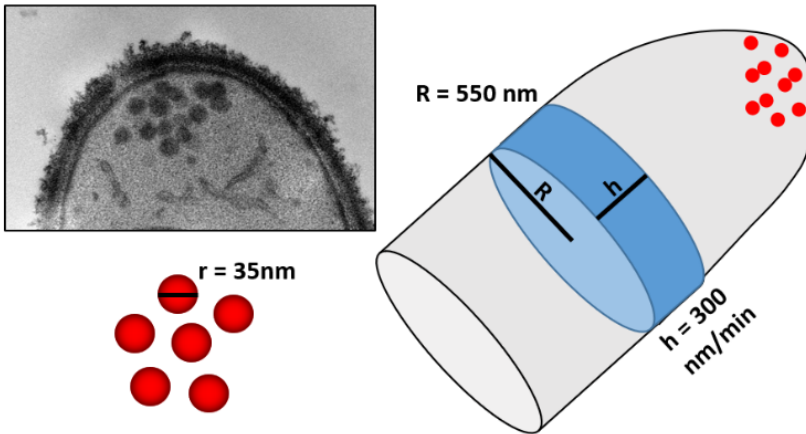
Geometrical parameters: SV radius (r), filament radius (R) and extension rate (h)

Modeling based on geometrical parameters.

In our calculation, the minimal rate of vesicle fusion is dependent only on the amount of membrane delivered by each vesicle (assuming that the SV population observed represents the sole contributor to extension), and the filament extension rate. We also assumed that vesicles transfer all their membrane to the PM during fusion. We modeled each SV as a sphere of radius of 35 nm, the filament as a cylinder of radius 550 nm (as quantified by ssTEM, ignoring the shape at the apex), and the C. *albicans* filament extension rate at 300 nm/min as determined elsewhere[1].

Known parameters from ssTEM:

1) SV diameter: 69.7 nm ± 10.7 nm (STD)

2) SV number at the apex: 57.75 ± 19 (STD)

3) Filament diameter approximated to 1100 nm

Other parameters:

1) Hyphal extension rate: 300 nm/min

Assumptions and calculation:

1) Assume SVs are perfect spheres.

2) Surface area of sphere of radius 35 nm represents membrane contribution of each SV to change in filament membrane surface area after SV fusion with plasma membrane

$A_{sphere} = 4\pi r^2$ r= 35 nm $A_{vesicle}$ = 15,393 nm^2 = 1.54x10^4

3) Assume filament is a perfect cylinder, calculate area added to filament per min.

$A_{cylinder} = 2\pi Rh$ R= 550 nm   h= 300 nm/min $A_{cylinder/min}$ = 1.03 x 10^6

$A_{cylinder/min} / A_{sphere} = 2\pi Rh/ 4\pi r_2 = Rh/2r^2 = 67.31$ vesicles/min= 1.12 vesicles/second

4) Number represents **the minimum rate of SV fusion with the plasma membrane required to provide new membrane for filament extension**.

5) Thus, **minimum time for SV contained in an average Spk to fuse with PM is**:

$$\frac{SV\ number/\ tip}{A_{cylinder/min}\ /\ A_{sphere}} = \frac{60}{67.31} = 0.89\ min/Spk = 53.4\ seconds/Spk$$

Reference

1.   Bassilana M, Hopkins J, Arkowitz RA. Regulation of the Cdc42/Cdc24 GTPase module during Candida albicans hyphal growth. *Eukaryot Cell*. 2005;4(3):588-603. doi:10.1128/EC.4.3.588-603.2005.

Figure S1. Nearest neighbor and distance to plasma membrane analysis. (A) The distance from each vesicle circumference to the circumference of its nearest neighbor was measured (n = 6 cells, 503 vesicle pairs). Negative values represent perceived vesicle overlap due to the TEM image being a projection of a 100 nm thick section that may contain two vesicles aligned in the Z axis. (B) The maximum distance between overlapping vesicles is calculated to be ~ 30 nm. (C) Distance between each vesicle and the nearest PM segment (n = 6 cells, 489 vesicles).

Figure S2. Cytochalasin A disrupts the integrity of the C. *albicans* secretory pathway domains. Cells were serum induced for 30 min followed by treatment with 10 μM cytochalasin A for 15 min. Cells were then fixed and examined by ssTEM. (A) Overview of hyphalfilament organization. (B) Two sections from the cell shown in panel A, showing tip organization. Elongated membranes and vesicles are highlighted in overlay. (C) Visualization of 3D features observed in B shown from different viewpoints.Colors represent: Internal membranes (yellow), SVs (red), mitochondria (green), lipid droplets (white). Scale bars are 1 μm in (A) and 500 nm in (B).
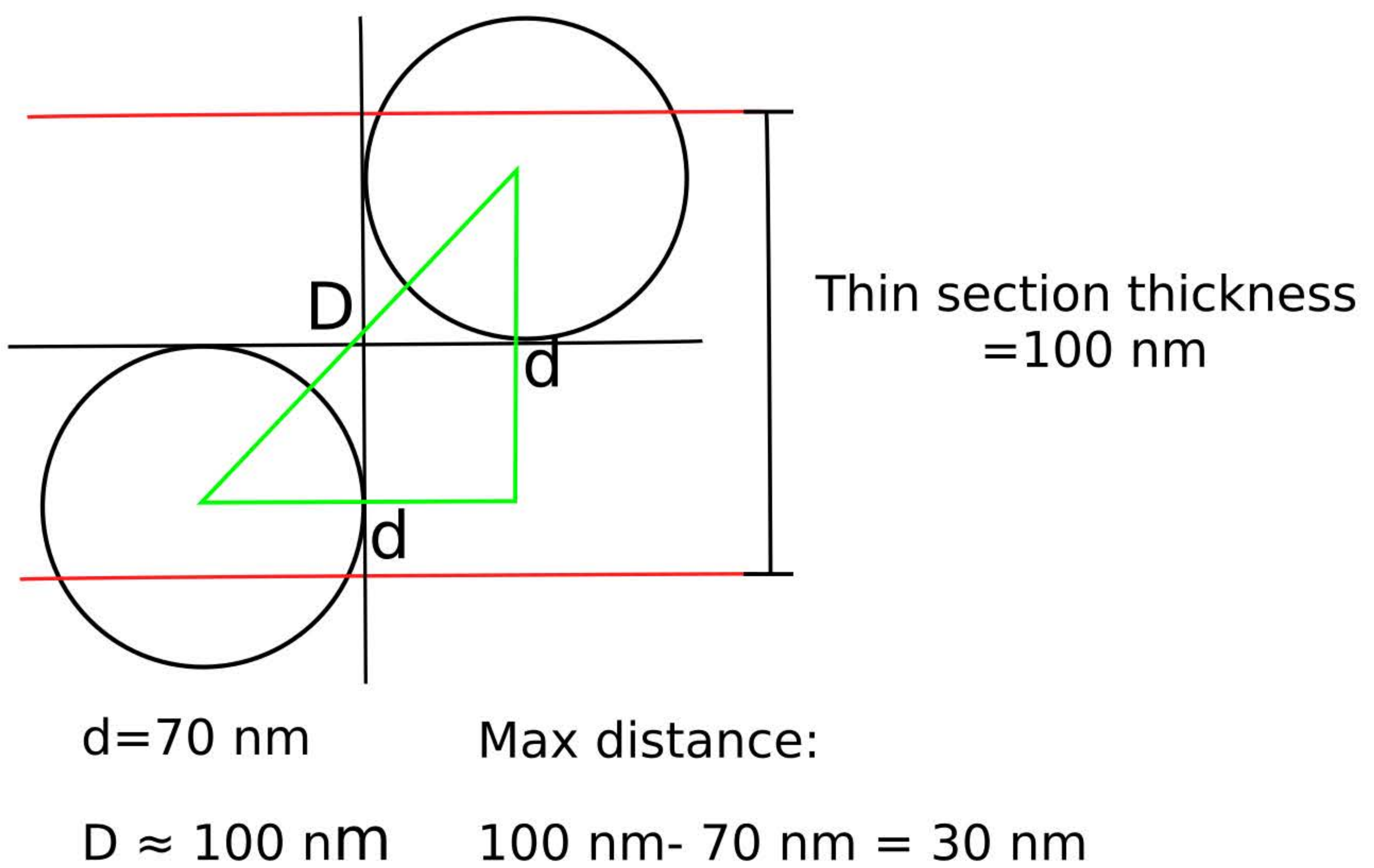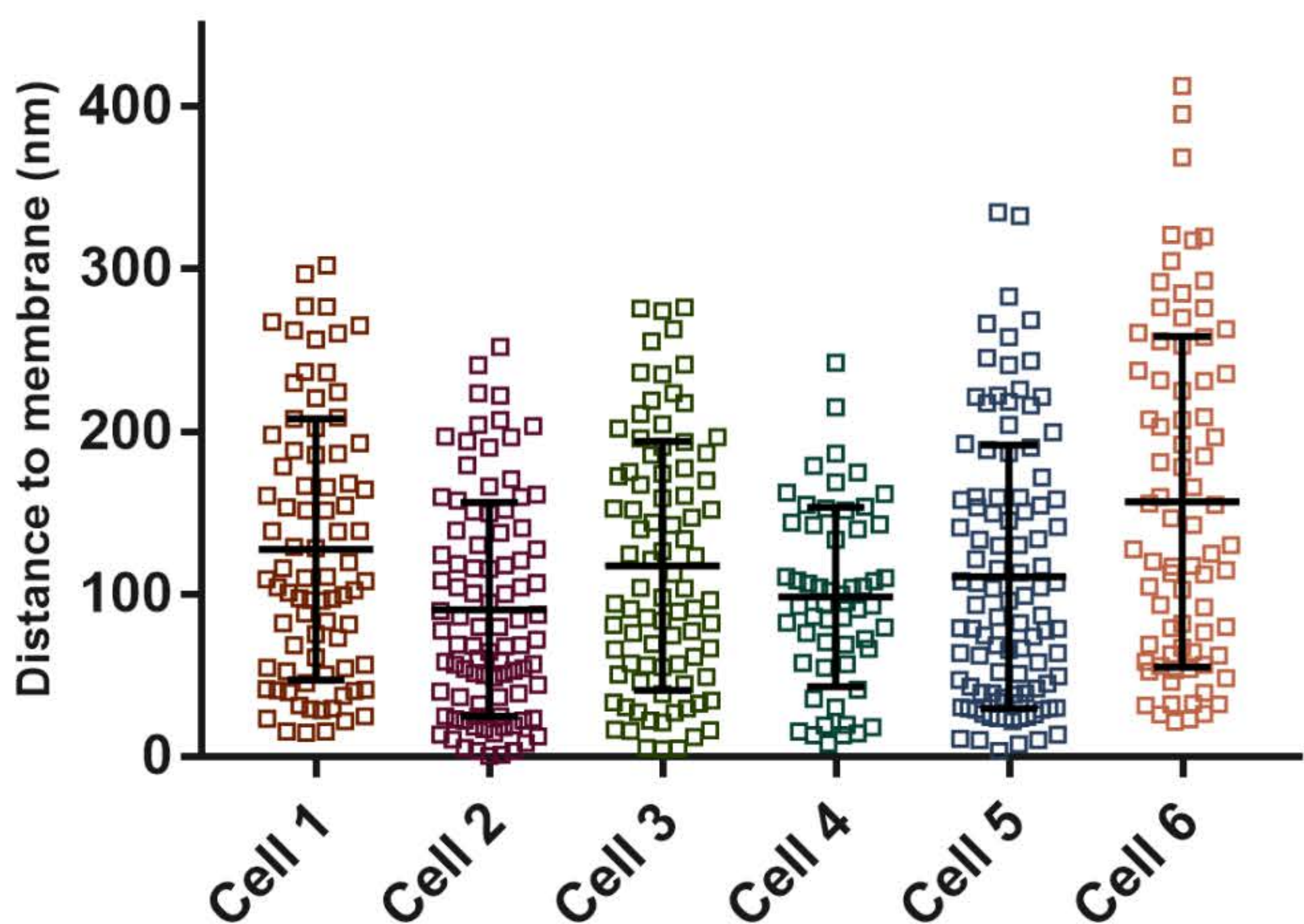
A

Nearest neighbour distance (nm)

Overlapping vesicles
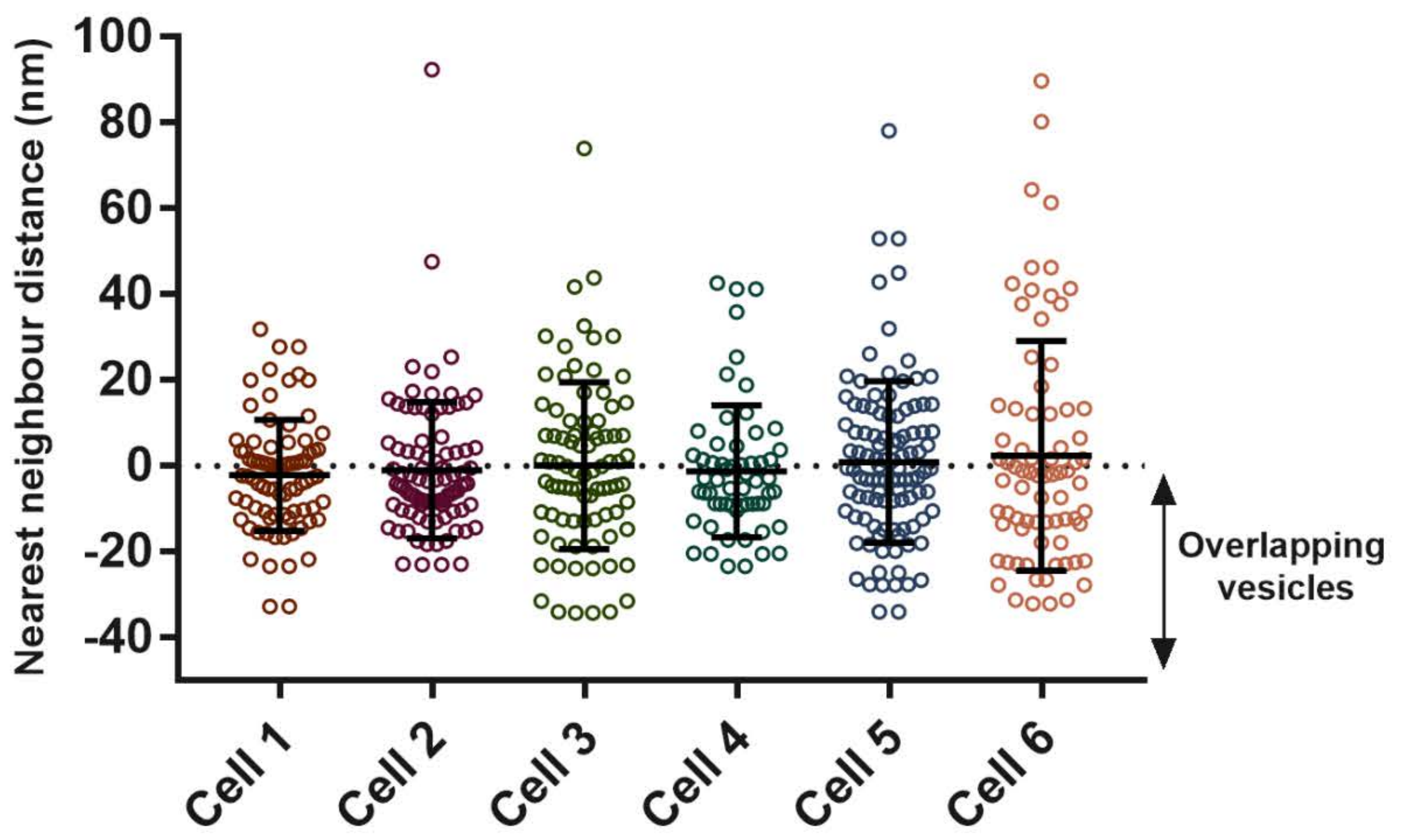
	Cell 1	Cell 2	Cell 3	Cell 4	Cell 5	Cell 6
Mean	-2.101	-0.9393	0.1471	-1.131	0.9888	2.465
Std. Deviation	12.94	15.85	19.41	15.38	18.79	26.75

	Cell 1	Cell 2	Cell 3	Cell 4	Cell 5	Cell 6
Median	-2.317	-4.411	-1.016	-3.436	-0.5972	-2.033
75% Percentile	3.769	4.197	10.46	3.87	11.72	13.39

B

Thin section thickness = 100 nm

d=70 nm

D ≈ 100 nm

Max distance:

100 nm- 70 nm = 30 nm

C

Distance to membrane (nm)

	Cell 1	Cell 2	Cell 3	Cell 4	Cell 5	Cell 6
Mean	127.8	90.62	117.7	98.37	110.8	156.9
Std. Deviation	80.27	65.78	76.45	55.09	81.12	101.5

	Cell 1	Cell 2	Cell 3	Cell 4	Cell 5	Cell 6
Minimum	14.66	0.4007	4.873	8.249	3.465	21.54
25% Percentile	54.79	36.8	52.97	60.02	39.2	64.04

Nuc